ORIGINAL PAPER

CrossMark

Characterizing Subsurface Archaeological Structures with Full Resolution 3D GPR at the Early Dynastic Foundations of Saqqara Necropolis, Egypt

Mahmoud Gaballah[1,2] · Mark Grasmueck[3] · Motoyuki Sato[4]

Abstract

Currently, Ground Penetrating Radar (GPR) used in archaeological prospection is based on 2-D parallel line methodologies characterized by line spacing from 0.25 to 1 m (common line separation is 0.5 m) with different GPR antennas and extensive interpolation used to fill data gaps. High resolution 3-D GPR images of the subsurface can be obtained by recording data with a quarter wavelength grid spacing in all directions. Recently, we used a new GPR system which is a combination of commercial GPR with a rotary laser positioning system developed at Tohoku University for full-resolution subsurface imaging. In this paper we will show how the high density 3-D GPR data acquired over an area of about 14 m×28 m can improve the image quality and reveal the subsurface archaeological structure of early dynastic foundations in the Saqqara area. The GPR vertical cross-sections and the horizontal depth slices extracted from the full-resolution 3-D GPR reveal great information about ancient human activities, most likely burial mounds. GPR data at depth greater than 1.3 m were overwhelmed by "ringing features" (repeated horizontal harmonic-like features) most probably caused by the presence of underlying shallow layers of low resistivity shale and claystone. A 2-D electric resistivity tomography (ERT) profile was acquired using a multi-electrode system with 1 m electrode spacing. The ERT section shows high resistivity for the near surface desert sand and gravel deposits. The second geoelectric layer detected by ERT shows a low resistivity value consistent with the presence of a highly conductive layer at a depth of about 1.3 m. Integration of such different geophysical tools (e.g. GPR with ERT) helps to interpret the repeated horizontal features in the 3-D GPR data.

Keywords 3D GPR · Rotary laser positioning system (RLPS) · Saqqara · Archaeology · Electric resistivity tomography · Full resolution

✉ Mahmoud Gaballah
   mahmoud_gabala@yahoo.com; m.abdelmawgoud@mu.edu.sa

Extended author information available on the last page of the article

1 Introduction

Archaeologists, geoscientists and engineers need high-resolution and clear images of the subsurface in order to understand how buried structure, rock, soil, water and life interact. Recently, conventional ground penetrating radar (GPR) used in archaeological prospection has been based on relatively widely-spaced, parallel 2-D survey profiles with line spacing ranges from 0.25 to 1 m with extensive interpolation used to fill data gaps. The resulting subsurface images can be displayed as fence diagrams or highly-interpolated pseudo 3-D image cubes [1]. Such GPR surveys do not exploit the full-resolution of GPR due to coarse grid spacing during data acquisition. Full-resolution imaging requires un-aliased recording of reflections and diffractions coupled with 3-D migration processing [2]. Full-resolution 3-D GPR imaging also needs antennae with a wide-open radiation cone (as much as ~ 60° radiation angle) and less than a quarter-wavelength grid spacing in all directions on the surveying surface [2]. Correlation between 2-D GPR sections separated by a distance that is much larger than the target size is doubtful and unfortunately too coarse to accurately resolve most subsurface structures [1]. Furthermore, the image includes too much ambiguity about the object geometry, and small targets cannot be detected.

Un-aliased 3-D GPR images of the shallow subsurface require spatially dense data sampling. The trace interval must be small enough to sample entire diffraction patterns in order to see small subsurface details [3].

Manual GPR surveying has been replaced for the most part by the use of some type of Global Positioning System (GPS). However, GPR data recording is much faster than the time required for accurate positioning using GPS [4, 5]. In addition, field terrain and/or structures may block line-of-sight to GPS satellites low on the horizon which are critical to accurate positioning.

For effective 3-D data acquisition, continuous centimetre-level coordinate precision over extended areas is very important. Currently, we use a new generation of GPR which combines a rotary laser positioning system (RLPS) with conventional GPR into a highly efficient and simple to use 3-D subsurface imaging system [6]. The laser positioning enables acquisition of continuous millimetre-level accuracy for x, y, and z coordinates simultaneously from a small detector attached to the moving GPR antennae (Fig. 1).

Impulse GPR antennae have an ultra-wide range of bandwidth with frequency range more than double antenna central frequency. High frequency signal content and steeply dipping diffraction tails are essential for horizontal resolution [7], which can be calculated after migration from the equation:

$$\Delta H_r = \frac{\lambda_{min}}{4 \sin \alpha_{max}}, \tag{1}$$

where ΔH_r is the minimum horizontally-resolvable distance, α_{max} is the steepest plane-wave angle used for migration, and λ_{min} is the minimum observed wavelength [8, 9].
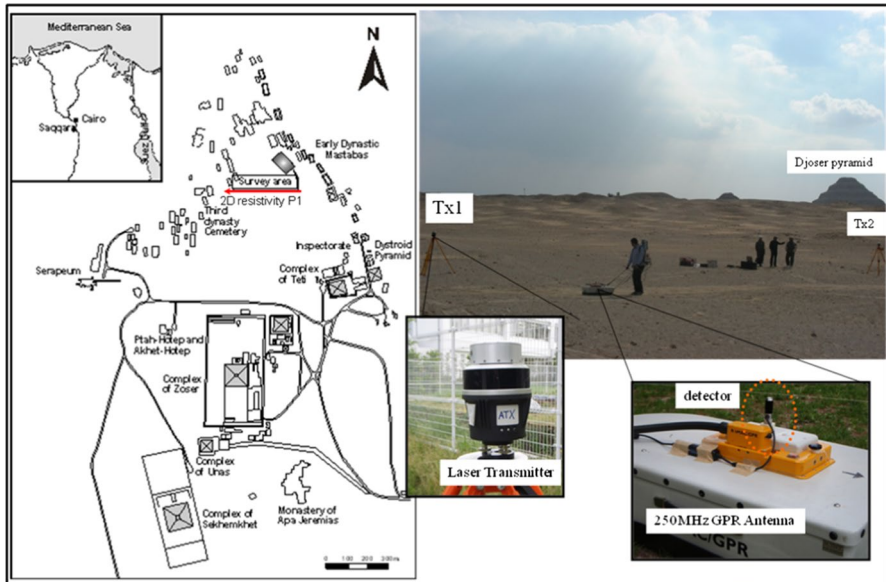
Fig. 1 Location map of the Saqqara area within Egypt. Survey site was located in the northern part of Saqqara. Top right image shows 3-D GPR system during data acquisition. Bottom right shows laser detector mounted on the 250 MHz GPR antenna. Red line on the map indicates the location of the 2-D geoelectric resistivity tomography (ERT) profile (Color figure online)

Proper sampling of a dipping plane wave requires trace spacing Δx to be equal or smaller than the Nyquist sampling intervals Δx_N [2, 3]:

$$\Delta x \leq \Delta x_N = \frac{\lambda}{4 \sin \alpha}, \tag{2}$$

where λ is the wavelength and α is the dip angle of the plane wave [2, 3]. For constant velocity and horizontal earth surface, the plane-wave angle is equal to the geologic dip of the corresponding plane reflector element and also equal to the antenna radiation pattern opening angle measured from the vertical. For angles of 60° (sin 60° = 0.87) and larger, the spatial Nyquist sampling interval quickly approaches a quarter-wavelength [2].

Recording such a dense full-resolution 3-D dataset requires less than a quarter-wavelength line spacing in all directions based on the un-aliased sampling criterion [2, 10]. In practical terms, this corresponds to 0.1 m grid spacing for a full-resolution 3-D GPR image with a 250 MHz center frequency antenna, and 0.05 m grid spacing for a 500 MHz antenna [6]. Table 1 indicates typical 3-D GPR grid spacing and corresponding coordinate precisions. As an example, grid spacing for an un-aliased 250 MHz antenna, GPR survey has to be less than 0.1 m, assuming subsurface velocity of about 0.1 m/ns [6].

Acquiring such dense data with conventional GPR systems takes too much time, and processing of such huge data is impractical, and requires special training. In

Table 1 Required grid spacing and coordinate precision for spatially un-aliased 3-D GPR survey assuming subsurface electromagnetic velocity of about 0.1 m/ns [6]

Frequency	100 MHz antenna (m)	250 MHz antenna (m)	500 MHz antenna (m)
Wavelength (λ) at 0.06–0.1 m/ns	0.6–0.1	0.24–0.4	0.12–0.2
Grid Spacing ($\lambda/4$)	0.15–0.25	0.06–0.1	0.03–0.05
Coordinate precision ($\lambda/8$)	0.075	0.03	0.015

addition, for efficient 3-D data acquisition, accurate and continuous recording of highly precise coordinates for the GPR antenna position over extended periods is important.

The objective of this paper is to introduce an applied field example of a new 3-D GPR system with full-resolution GPR to reveal the subsurface archaeological structure in the Saqqara area, Giza, Egypt (Fig. 1). To achieve our objective, a laser positioning 3-D GPR developed at Tohoku University, was used to image the subsurface archaeological remains in the north Saqqara site. A 2-D electrical resistivity tomography (ERT) survey was used to detect the shallow subsurface geologic setting since GPR data was suffering from high attenuation and ringing in the shallow part of the section (depths less than about 1.3 m).

2 Saqqara Archaeological Background

Egypt contains many valuable monuments distributed throughout the country. A large number of these archaeological remains are still buried beneath shallow veneers of unconsolidated sediments. Saqqara necropolis is located on the plateau at the eastern edge of the Western Desert, opposite the ancient Egyptian capital of Memphis. This great archaeological cemetery was one of the important burial sites for royalty and high-level government officials from the Early Dynastic period [11, 12].

The cemetery at Saqqara is one of the most important archaeological sites in Egypt. Over 6 km long, it contains thousands of underground burial sites, as well as the step Djoser pyramid which is the oldest known Egyptian pyramid [13–15]. In Djoser cemetery, to the north and west of the Djoser pyramid complex, several tombs were built during the 3rd Dynasty and later [16, 17]. Among these tombs, the mastaba of Ptahhotep of the 5th Dynasty is the most famous (mastabas are large rectangular structures built for the funerals and burials of the earliest Pharaohs). To the west of this cemetery, a gallery of tombs for the sacred bulls of Apis, recognized today by its Greek name Serapeum, was constructed from the 19th Dynasty on. It would continue to be used until well into the Roman Period.

Most of the Saqqara necropolis is covered by a thin layer of sand overlying horizontal to sub-horizontal layers of limestone with intercalations of marl, cross-bedded sandstone, conglomerate, shale and claystone [18]. The current investigation is focused on the interior of a large Early Dynastic mastaba situated along the

north-eastern edge of the Saqqara necropolis (Fig. 1). The interior of the mastaba covers a large area and is surrounded by a sun-dried mud-brick wall that ranges from 0.5 m to 2 m thick and varies in height from a few centimeters to more than 2.5 m. Within the mastaba, there are a number of shafts and a small remnant of an inner mud-brick wall (Fig. 2). Several of the shafts are open to the surface. Some have an interior facing of mud bricks or limestone blocks, whereas others are simply-designed holes. At the base of several open shafts, with diameters from 2 m to more than 4 m and depths of 1 m to 5 m, there are small rooms and blocked-off tunnels [17].

3 3D GPR Data Acquisition and Field Site Description

The strategy of our survey involved acquisition of GPR data consisting of densely-spaced 3-D GPR over areas of suspected subsurface archaeological remains. For example, grid spacing for a spatially un-aliased 250 MHz GPR survey must be 0.1 m or less assuming 0.1 m/ns electromagnetic subsurface wave velocity [2, 3, 19]. The survey was completed by collecting 3-D GPR datasets which were begun at regular time intervals, and acquired in the same profile sequence at an average antenna speed of 0.5 m/s. Acquiring such dense data sets in the field is one of the main bottlenecks preventing wide use of high-quality 3-D imaging. Today's commercial GPR systems are only capable of efficiently collecting widely spaced 2-D profiles that can be displayed as fence diagrams or highly-interpolated pseudo-3-D image cubes. The challenge in producing sharp full-resolution 3-D image cubes is to acquire data with a continuously-moving GPR antennae while obtaining millimeter-precision coordinates for every radar trace recorded as the antennae is towed along tightly-spaced lines in a "lawnmower" pattern.

A novel rotary laser positioning system (RLPS) technology was integrated with GPR (Fig. 3a) into a highly-efficient and simple to use 3-D imaging system [6]. The new system in Fig. 3a enables acquisition of coordinates with

(a)   (b)

Fig. 2 Photographs showing some archaeological features near the survey site. **a** View of mastaba with surrounding mud walls, **b** several open shafts
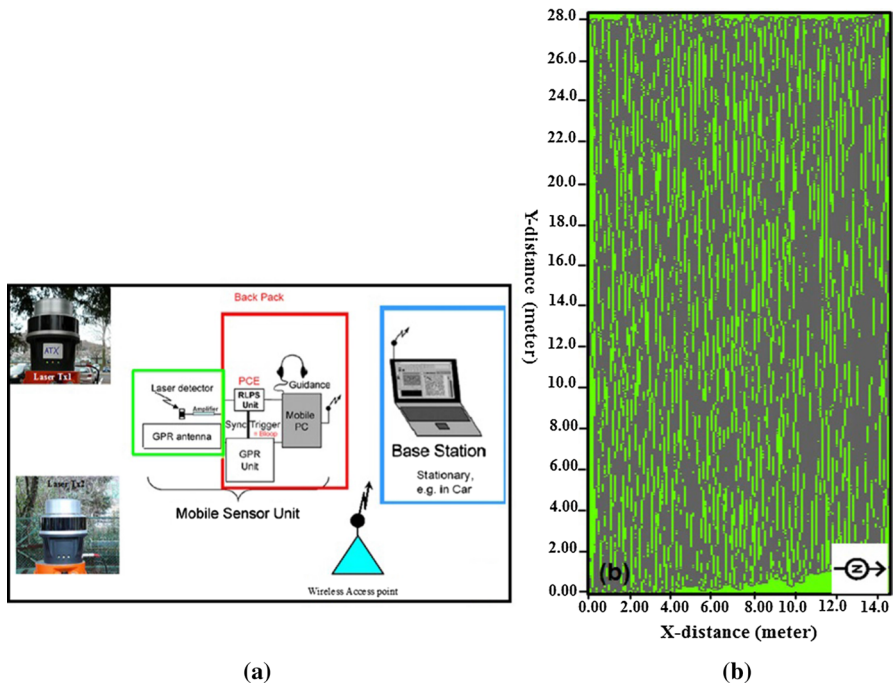
Fig. 3 **a** Schematic diagram showing the 3-D GPR system, where the base station is wirelessly connected to the mobile sensor unit controlling both GPR and RLPS. **b** Plot of survey tracks generated in real time during 3-D GPR data acquisition. Antenna turn-arounds are visible at the east and west ends of the survey area

millimeter-precision in x, y, and z using a small detector attached to the moving GPR antennae. Laser coordinates streaming with 20 updates per second from the detector are fused in real time with the GPR data (Fig. 3b). A real detector attached to the moving GPR antenna detects and processes signals from each visible transmitter, initial processing consists simply of measuring the time between laser strikes and the time between the last laser strike and the strobe, which simply known as intervals. Given the angular information from at least two transmitters and provided with the position and orientation of each transmitter, a unique 3D position within the measurement volume can be calculated [20]. This position calculation is synchronized with GPR trace and both are recorded on the computer at the mobile sensor unit (Fig. 3a). The person moving with GPR antenna is automatically guided by LED array elements along pre-computed tracks following a dense lawnmower pattern with 0.1 m inline spacing to acquire parallel GPR profiles. For all of the surveys reported here, we used a shielded bistatic 250 MHz GPR antenna and a CU-II control unit [21], modified for integration with the RLPS. Antenna offset between transmitter and receiver was 0.36 m, and we recorded 602 samples per trace, with eight stacks, and a sampling interval of 0.325 ns using a sampling frequency of 3941 MHz resulted in a maximum

two-way travel time of about 193 ns [21]. Figure 3b shows a plot of survey tracks generated in real time at the base station laptop during 3-D GPR data acquisition. Antenna turn-arounds are visible at the east and west ends of the survey area.

The survey area for this study was about 14.6 m × 28.2 m, on friable desert sand in the north Saqqara site on the plateau area (Fig. 1). Three persons completed the 3-D GPR survey in less than eight hours, recording about 82,908 radar traces at 0.05 m intervals covering the entire area along with 147 parallel east–west inlines spaced by 0.1 m apart.

A 2-D electrical resistivity tomography (ERT) survey was used to investigate the subsurface resistivity distribution and geologic stratigraphy beneath part of the site. The resistivity method is based on measuring the electrical potential which results from an applied direct electrical current flowing in the ground. The resistivity section was acquired using a SYSCAL-R2 multi-electrode system recording 278 resistivity readings of Wenner–Schlumberger configuration. A set of 32 electrodes with 1.0 m spacing attached to intelligent nodes generated a 31 m profile with about 4.8 m effective survey depth with complete data coverage in the center third of the section.

4 Data Processing

All 3-D GPR datasets were processed in exactly the same way. The processing sequence is shown in Fig. 4, and is based on a combination of processing modules developed in LabView (National Instruments) [6, 22, 23]. The processing steps are as follows: (1) ''Data fusion'' assigns laser-derived x, y, and z coordinates to each radar trace acquired. As a result, the GPR track lines can be plotted on a map. (2) ''Detrending'' compensates for zero time drift due to temperature changes affecting the GPR electronics by automatic picking of first breaks. The spatially smoothed differences between the first break picks and a reference first break time are applied as vertical time shifts to traces. The smoothing is applied to reduce the effect of random first break jitter. This step also removes zero time shifts between

**Fig. 4** Processing sequence applied to all 3-D GPR data [6]
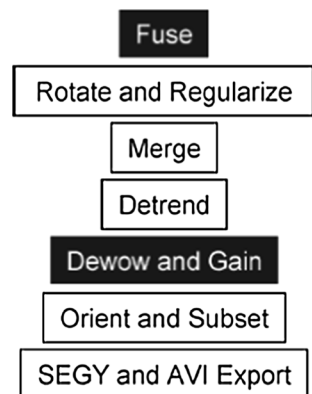
individually-recorded data sets aligning all first breaks to one common level throughout whole survey. (3) The zero time is adjusted by delaying the first break by the time it takes the direct airwave to travel from transmitter to receiver. (4) The ''dewow'' step [24], removes very low frequency components of the data associated with either inductive phenomena for possible instrumentation dynamic range limitations and/or analog-to-digital conversion. The GPR receiver and transmitter antenna are very close; therefore, the field near the transmitter contains low-frequency energy associated with electrostatic and inductive fields, which decay rapidly with distance. This low frequency energy often yields a slowly time-varying component to the measured field data. This energy causes the base level of the received signal to bow up or down. This signal processing step is referred to as "dewow" [25]. (5) The same gain curve is applied to all data acquired within different datasets. Radar signals attenuated very rapidly with depth so that, signals from greater depths are very small when compared to signals from near surface. There are various ways of applying time gain to radar data. Gain should be selected based on physical model, not a user whim, with the objective of minimizing artifacts created by the process [25]. The applied gain curve is based on a smoothed Hilbert transform (HT) of a representative set of traces extracted from the 3D survey data volume. (6) Regularization populates an identical 0.05 m×0.01 m bin grid for all surveys with the nearest available trace. (7) Velocity estimates are based on diffraction hyperbola analysis with ReflexW from Sandmeier Scientific Software [26]. Figures 5 and 6 show typical 2-D GPR vertical cross-sections of processed data extracted from the 3-D GPR

Inline #1 at start position
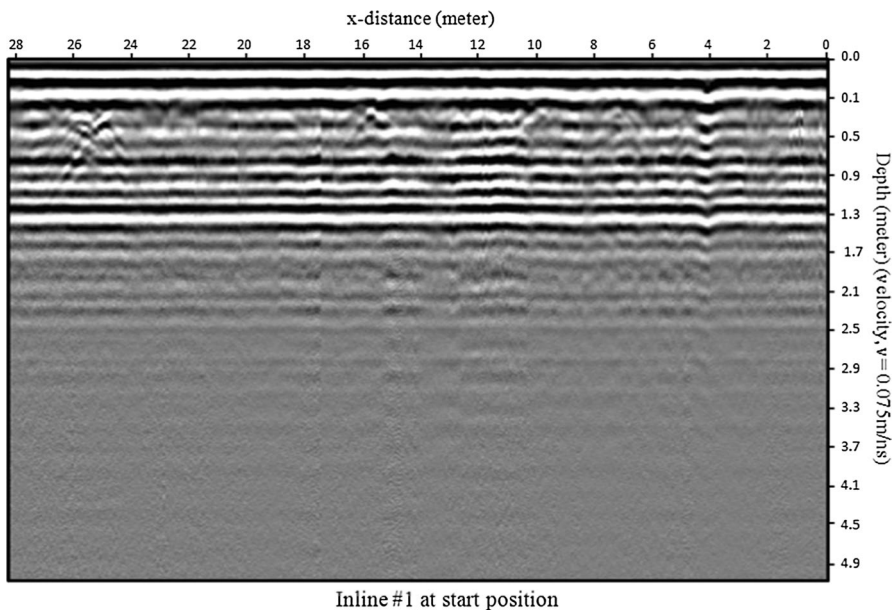
Fig. 5 A 2-D GPR vertical cross-section of processed data extracted from the 3-D GPR data cube at×distance 1.0 m. Many hyperbolic reflections can be seen at depth of about 0.2 m
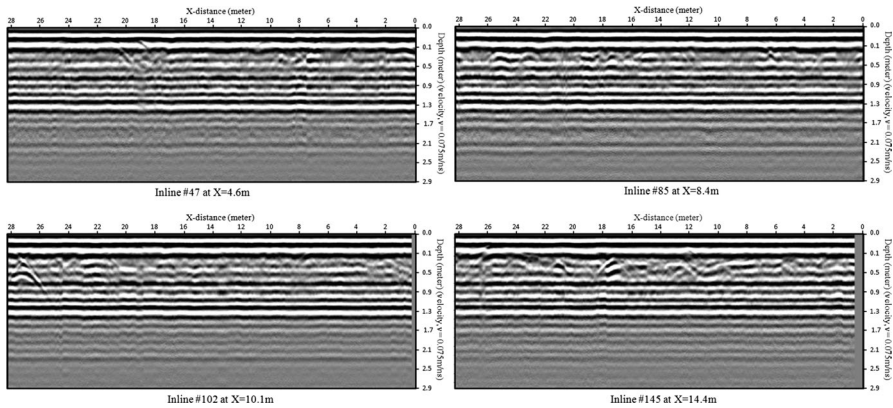
Fig. 6 Succession of selected 2-D GPR vertical cross-sections extracted from 3-D GPR data cube. Due to space limitation only four GPR profiles are shown here. Several diffraction hyperbola originated from subsurface archaeological features are easily observable at depths between 0.2 and 1.3 m. Hyperbola shape and dimensions are a function of target size and define a circular pattern on the horizontal time-slices

data cube, in which we could observe many hyperbolic reflection patterns related to the near-surface archaeological structures similar to those in Fig. 2.

Geoelectric field data were processed using the software RES2DINV [27]. This software calculates the true resistivity model by inverting the apparent resistivities measured along the profile. The goodness of fit between the measured apparent resistivities and the model apparent resistivities predicted by the true resistivity model are expressed as the root mean square (RMS) error between the observed and predicted pseudosections. The non-linear inversion is run through several iterations that progressively minimize the RMS error using a least-squares algorithm technique to produce the models (Fig. 7) [28]. Interpretation of the inverted model of the electrical resistivity profile is based on resistivity values and borehole data shown in (Fig. 8).

5 Result and Interpretation

Most of the Saqqara tombs are built with sun-dried mud-bricks walls (Fig. 2a) with a thickness of about half a meter, and with different heights ranging from a few centimeters to more than 2 m. Most of these tombs are still buried under a thin layer of the desert sand. Within mastaba tombs, there are a number of shafts (Fig. 2b) and small remnants of inner mud-bricks walls visible on the ground surface.

Interpretation of the 2-D vertical cross-sections (Fig. 6) extracted from the 3-D GPR data cube show numerous hyperbolic reflections to a depth of about 1.3 m from the near surface mud bricks walls, which can be easily observed during data acquisition. These hyperbolic features produce the circular pattern on the horizontal time-slices (Fig. 9).

(a)

(b)
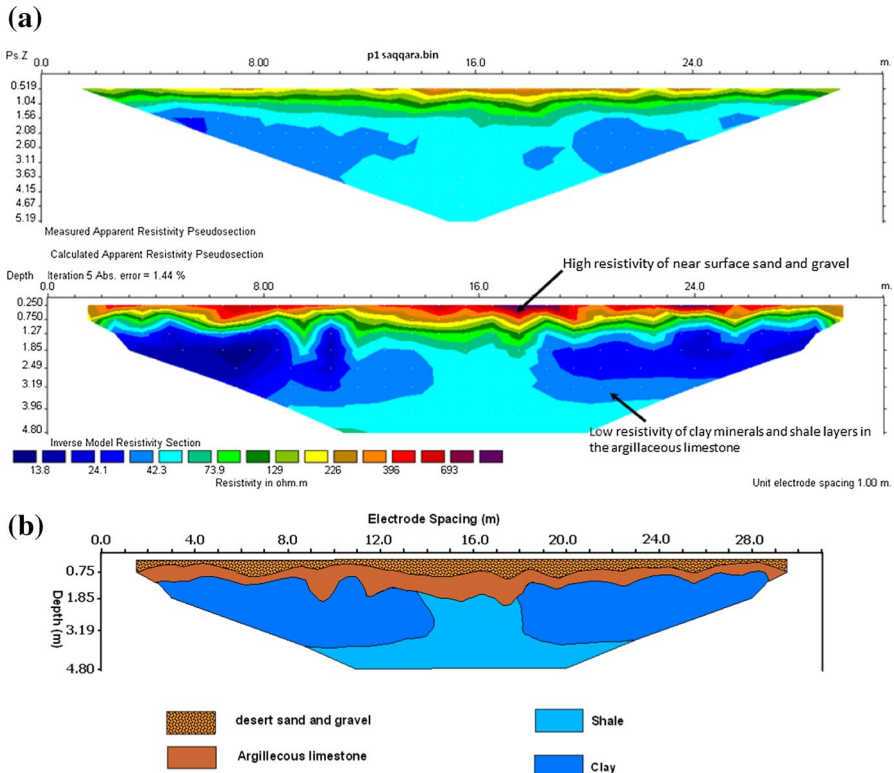
Fig. 7 2-D ERT section acquired with Wenner–Schlumberger configuration. A set of 32 electrodes with 1.0 m electrode spacing generate a 31.0 m profile length with about 4.8 m depth of data coverage in the center of the profile. **a** The measured (top) and inverted (bottom) of the electrical resistivity profile, **b** geologic interpretation based on resistivity values and borehole data

Time slice images show three main types of reflections: large distinct circular features (targets with sectors A, D, F, G) visible through time-slice as in Fig. 10 (A and F about 7 m × 7 m, while D and G is about 5 m × 5 m). These are probably associated with ancient temple base remains. These circular scattered anomalies aligned into well-defined features that give the impression that they are associated with subsurface archaeological structures. However, the number of anomalies and the dimensions of the large structure they represent are still hard to interpret.

A very distinct circular feature in the amplitude slice as in Fig. 10a, b, d (features with name B, C, E, H, I) are mostly compatible (both in shape and dimensions) with the shafts discovered in the excavated site shown in Fig. 2.

Small circular features shown in the time-slice image at a depth of about 0.8 m (Fig. 10d, e) probably originate from rubble anomalies scattered in the near surface sand and gravel. Exploration indicates that many tombs close to our survey site suffered from robbery as could be observed on the surface. Buried in the soil,
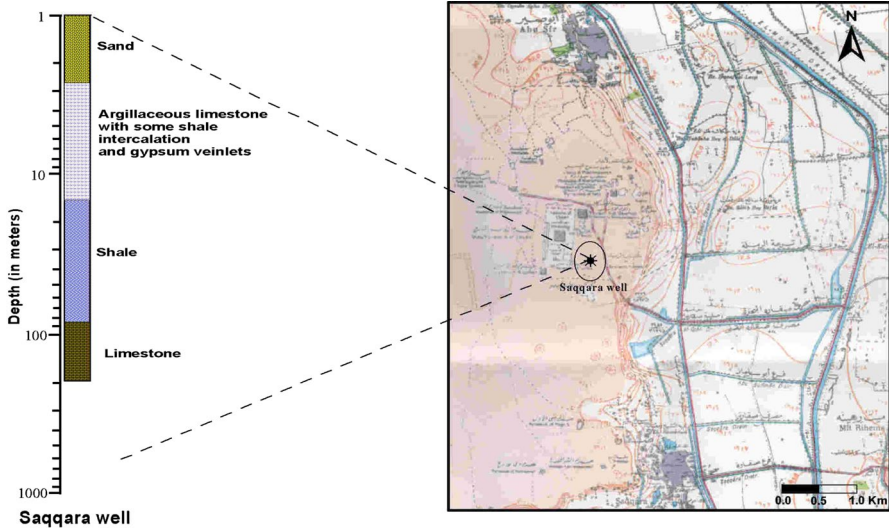
Fig. 8 Location and lithological description of Saqqara well (Modified after Egyptian Supreme Council of Antiquities)
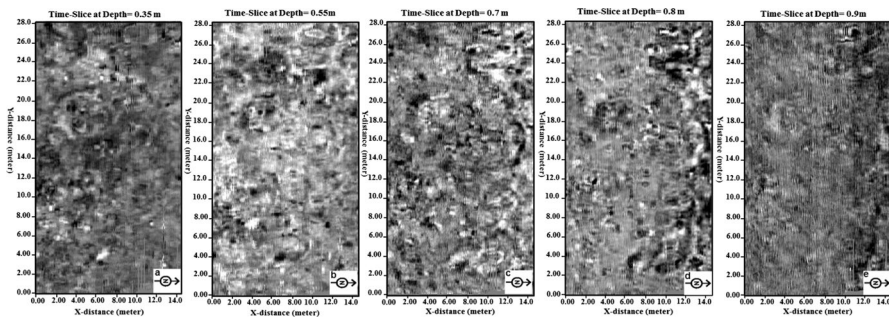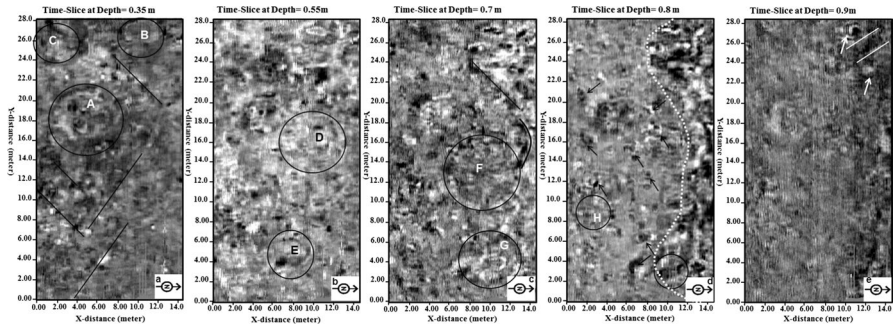

Fig. 9 Horizontal time-slice images obtained from 3-D GPR data with inline spacing 0.1 m at different times/depths

there appears to be a network of straight parallel elongated lines (Fig. 10a) possibly caused by large street structures between ancient buildings.

The horizontal time-slice at depth of about 0.8 m (Fig. 10d) shows possible archaeological complex features which appeared as elongated and large structures with high amplitude reflections at the most right part of the slice (highlighted with white dashed line from top to bottom in Fig. 10d), which exhibits a great contrast between there outer edge margins and the surroundings.

GPR profiles (Fig. 6), extracted from different locations in the data cube, and the time slice image as well, at depth of about 1.3 m are overwhelmed by "ringing features" (repeated horizontal harmonic-like features). In order to understand the reason for GPR ringing feature and the high attenuation of GPR signals, a 2-D

Fig. 10 Interpretation of time-slice images obtained from 3-D GPR data cube at depths 0.35, 0.55, 0.7, 0.8, and 0.9 m, respectively. The circular shapes indicate subsurface anomalies associated with the hyperbolic reflection events from near surface archaeological targets

electric resistivity tomography profile was acquired with a multi-electrode array and the results were displayed as a two-dimensional variation of inverted model resistivity. Figure 7a shows the 2-D ERT section and its interpretation (Fig. 7b) which are based on resistivity values and the borehole data in Fig. 8. The upper part of the section shows high resistivity (> 226 Ωm) for the near-surface desert sand and gravel deposits. Whereas, the areas showing lower values (between 74 Ωm to < 226 Ωm), are probably related to the argillaceous limestone layer.

The third layer detected by ERT survey appears as low resistivity values consistent with the presence of clay and shale horizons in the argillaceous limestone at a depth of about 1.3 m from the surface. Resistivity values from 1 to 25 Ωm are probably related to clay while the section (Fig. 7) at depth of about 1.8 m is dominant by resistivity of about 42 Ωm corresponding to shale layers. The presence of the sub-horizontal layer of shale and clay layers intercalated with argillaceous limestone [18], prevented GPR signal from penetrating deeper than 1.3 m for the 250 MHz antenna.

There are many references [i.e. 29, 30] indicating that GPR signal penetration decreases significantly for 100 MHz antenna once the resistivity of the surface sediments drops below about 30 Ωm. In the northern Sahara desert of Tunisia, [31] experienced a similar problem of very shallow depth penetration along many GPR profiles due to low resistivity of high percentage gypsum-rich-sands within the sand sediments.

6 Conclusions: What We Have Learned and Gained-Some Rules of Thumb

Our survey example shows how full-resolution 3D GPR is capable of generating high-resolution and intuitive subsurface views of complex archaeological structures at Saqqara Necropolis. Such dense grid data with fast 3-D acquisition equipment, plus accurate positioning system are important for revealing subsurface

archaeological structures. The dense grid spacing used for this survey provide the necessary basis for accurate description of 3-D internal archaeological foundations.

Probably the most important thing that we learned from this study was the practicality and maneuverability in high density GPR data acquisition in a short time. When we began the survey, we knew data acquisition needed to be dense enough to image the archaeological features buried beneath the preserving fill. We also wanted to show how un-interpretable GPR images can be transformed into clear images of shallow subsurface structure. When approaching a large area, such high-density data acquisition with standard commercial GPR system is not practical and takes too long (at least 2 days were needed to cover the whole area with 4 persons in the field). Furthermore the data are difficult to process, and require an immense investment of time and energy. However, noninvasively imaging of features guides archaeologists to interesting spots for excavations, so an efficient and practical GPR method is very important.

Ringing is a term usually used in GPR community for signals that reverberate in a general fashion. Such GPR responses are created when a GPR signals interact with an object in such a way that the signal repeatedly bounces around within an object or between two or more objects. Sources of ringing in GPR measurements are many, with the most common source being induced current running back and forth on a metal object or a highly conductive layer. ERT data help to resolve the ambiguities in the interpretation of the ringing in GPR data by indicating the presence of highly conductive shale layers. In fact, the knowledge of target resistivity and subsurface geologic conditions allows us to properly understand and interpret the reasons for the repeated horizontal features in the 3-D GPR data with the 250 MHz antenna. We believe that if a lower frequency antenna was used, deeper imaging for subsurface archaeological structures would be possible.

References

1. Novo, A., Grasmueck, M., Viggiano, D., & Lorenzo, H. (2008). 3D GPR in archeology: What can be gained from dense data acquisition and processing?. In *12th international conference on ground penetrating radar 2008*, Birmingham, UK.
2. Grasmueck, M., Weger, R., & Horstmeyer, H. (2005). Full-resolution 3-D GPR imaging. *Geophysics, 70*(1), K12–K19.
3. Grasmueck, M., Weger, R., & Horstmeyer, H. (2003). How dense is dense enough for a ''real'' 3D GPR survey? In *Society of exploration geophysicists, 73rd annual international meeting, expanded abstracts* (pp. 1180–1183).
4. Lehmann, F., & Green, A. G. (1999). Semiautomated georadar data acquisition in three dimensions. *Geophysics, 64*(3), 719–731.
5. Young, R., & Lord, N. (2002). A hybrid laser-tracking/GPS location method allowing GPR acquisition in rugged terrain". *The Leading Edge, 21*(5), 486–490.

6. Grasmueck, M., & Viggiano, D. (2007). Integration of ground-penetrating radar and laser position sensors for real-time 3-D data fusion. *IEEE Transactions on GeoScience and Remote Sensing*, *45*(1), 130–137.

7. Claerbout, J. F. (1976). *Fundamentals of geophysical data processing*. New York City: McGraw-Hill Book Co., Inc.

8. Denham, L. R. (1981). Extending the resolution of seismic reflection exploration. *Journal Canadian Society of Exploration Geophysicists, 17,* 43–54.

9. Ebrom, D. A., Li, X. H., McDonald, J. A., & Lu, L. (1995). Bin spacing in land 3-D seismic surveys and horizontal resolution in time slices. *The Leading Edge, 14,* 37–40.

10. Yilmaz, O. (2001). *Seismic data analysis* (Vol. 1). Tulsa: Society of Exploration Geophysics.

11. Baines, J., & Malek, J. (1992). *Atlas of ancient Egypt*. Oxford: Andromeda.

12. Black, A. C., & Norton, W. W. (1993). *Blue guide Egypt*. London: Bedford.

13. Kinnaer, J. (2003). *The Ancient Egyptian Site*. https://www.ancient-egypt.org/index.html. Accessed Mar 2010.

14. Raffaele, F. (2003). *Early Dynastic Egypt*. http://members.xoom.virgilio.it/francescoraf/index.html. Accessed Mar 2010.

15. Sitek, D. (2003). *Ancient Egypt: History and chronology*. http://www.narmer.pl/indexen.html. Accessed June 2010.

16. Metwaly, M. (2004). *Geophysical contribution for inspection and protection of archaeological remains at Saqqara area, Egypt* (pp. 89–93). Ph.D. Dissertation, Faculty of Science, Mansoura University, Egypt, 2004.

17. Metwaly, M., Green, A. G., Horstmeyer, H., Maurer, H., Abbas, M., & Hassaneen, A Gh. (2005). Combined seismic tomographic and ultrashallow seismic reflection study of an Early Dynastic Mastaba, Saqqara, Egypt. *Archaeological Prospection, 12,* 245–256.

18. Said, R. (1990). *The geology of Egypt*. Rotterdam: Balkema.

19. Marchesini, P., & Grasmueck, M. (2015). The impact of high-density spatial sampling versus antenna orientation on 3D GPR fracture imaging. *Near Surface Geophysics, 13*(2), 197–207. https://doi.org/10.3997/1873-0604.2015007.

20. Metris (formerly Arc Second). (2006). *WorkSpace advanced metrology edition user's guide*. http://www.indoorgps.com. Accessed Nov 2008.

21. Mala Geoscience, A. B. (2005). *Product literature*. http://www.malags.se. Accessed Oct 2006.

22. National Instruments, Corp. (2005), *Product literature*. http://www.ni.com. Accessed Sept 2008.

23. Grasmueck, M., Moser, T. J., Pelissier, M. A., Pajchel, J., & Pomar, K. (2015). Diffraction signatures of fracture intersections. *Interpretation, 3*(1), SF55–SF68. https://doi.org/10.1190/int-2014-0086.1.

24. Annan, A. P. (2003). Ground penetrating radar principles, procedures and applications. Mississauga, ON, Canada. *Sensors and Software, 2003,* 278.

25. Harry, M. J., (2009), Chapter 1: Electromagnetic Principles of Ground Penetrating Radar. In A. P. Annan (Ed.), *Ground penetrating radar: Theory and applications. Elsevier Science* (1st Edn.). Amsterdam: Elsevier.

26. REFLEX Software. (2012). Sandmeier Scientific Software, Karlsruhe, Germany.

27. Loke, M. H., & Barker, R. D. (1996). Rapid least-squares inversion of apparent resistivity pseudosections by a quasi-Newton method. *Geophysical Prospecting, 44,* 131–152.

28. Loke, M. H. (2001). *Electrical imaging surveys for environmental and engineering studies. A practical guide to 2-D and 3-D surveys: RES2DINV Manual, IRIS Instruments*. www.iris-instruments.com.

29. Green, A. G., Lanz, E., Maurer, H., & Boerner, D. (1999). A template for geophysical investigations of a small landfill. *The Leading Edge, 18,* 248–254.

30. De Iaco, R., Green, A. G., & Horstmeyer, H. (2000). Integrated Geophysical Study of a landfill and its host sediments. *European Journal of Environmental and Engineering Geophysics, 4,* 223–263.

31. Lehmann, F., Horstmeyer, H., Green, A. G., Sexton, J., & Coulybaly, M. (1996). Georadar data from the northern Sahara desert: Problems and processing strategies. In *Proceedings of the 6th international conference on ground penetrating radar*, Sendai, Japan (pp. 51–56).

Affiliations

Mahmoud Gaballah[1,2] · Mark Grasmueck[3] · Motoyuki Sato[4]

Mark Grasmueck
mgrasmueck@rsmas.miami.edu

Motoyuki Sato
sato@cneas.tohoku.ac.jp

[1]　National Research Institute of Astronomy and Geophysics (NRIAG), Helwan, Cairo 11421, Egypt

[2]　Physics Department, College of Science and Humanities in Hawtet Sudair, Majmaah University, Majmaah 11952, Saudi Arabia

[3]　Marine Geology and Geophysics, RSMAS University of Miami, 4600 Rickenbacker Causeway, Miami, FL 33149, USA

[4]　Center for Northeast Asian Studies, 41 Kawauchi, Aoba-Ku, Sendai, Miyagi 980-8576, Japan